Dalton Transactions

An international journal of inorganic chemistry

Accepted Manuscript

This article can be cited before page numbers have been issued, to do this please use: C. Jatmika, K. Goshima, K. Wakabayashi, N. Akiyama, S. Hirota and T. Matsuo, *Dalton Trans.*, 2020, DOI: 10.1039/D0DT02353A.

ROYAL SOCIETY OF CHEMISTRY

rsc.li/dalton

View Article Online
DOI: 10.1039/D0DT02353A

Second-coordination sphere effects on reactivities of Hoveyda–Grubbs-type catalysts: A ligand exchange study using phenolic moiety-functionalized ligands

Received 00th January 20xx,
Accepted 00th January 20xx

DOI: 10.1039/x0xx00000x

Catur Jatmika, Kenta Goshima, Kazumo Wakabayashi, Naoki Akiyama, Shun Hirota and Takashi Matsuo*

The Hoveyda–Grubbs (HG) second-generation catalyst (HG-II), a Ru complex with 2-isopropoxybenzylidene ligand, is extensively used for olefin metathesis, the rearrangement of carbon–carbon double bonds. A well-known strategy to control its complex reactivity is to modify the phenyl ring in the ligand, thereby directly influencing the coordination of the phenolic oxygen to the metal center. We, herein, report that a functional group attached to phenolic moiety in 2-alkoxybenzylidene ligand can indirectly affect the reactivities of HG-type complexes. In this work, the ligand exchange reactions between HG-II and the phenolic moiety-modified 2-alkoxybenzylidene ligands are useful for evaluating the structural effects of the ligands. Specifically, an ethylene amide or an ester group at the terminal phenolic moiety in the benzylidene ligand was found to influence the relative stabilities of HG-type complexes to HG-II complex. The structural analyses proved that the observed effects of the functional groups on the complex staibilities originate from the interactions with a chlorido ligand in HG-type complexes without changes in coordination fashions at the metal centers. It was found that the outer-sphere interactions also influence the catalytic activities of HG-type complexes. Namely, the properties of HG-type complexes can be controlled by outer-sphere structural factors toward the metal center (*i.e.,* "second-coordination sphere effect"). In the design of functionalized HG-type complexes, the outer-sphere structural effects are to be considered in addition to the optimization of the metal coordination site.

Introduction

Both in the laboratory-level syntheses and industrial production of fine chemicals, olefin metathesis, the rearrangement of carbon–carbon double bonds, has gained increased methodological importance for forming the skeletons of natural products and pharmaceuticals in the presence of various functional groups in the starting compounds.[1, 2] Ru complexes, with Grubbs catalysts[3] as representative examples, are extensively used metal catalysts for olefin metathesis, because the metal complexes typically have high catalytic reactivities with appropriate stabilities. The high affinity of a Ru center toward olefins is also highly advantageous to regioselective syntheses.[4, 5] Particularly, the Hoveyda–Grubbs (HG) second-generation catalyst (HG-II (**1**), see Fig. 1(a)) has frequently been a research objective to investigate the structure-reactivity relationship. This is because the *N*-heterocyclic carbene (NHC) and 2-alkoxybenzylidene ligands in HG-type complexes not only contribute to the suitability of their stabilities but also enable introducing various structural modifications in these ligands.[6-8]

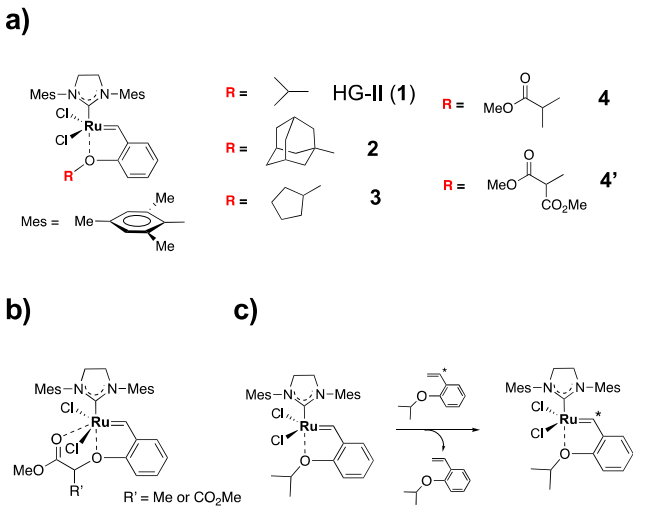

Fig. 1. (a) Chemical structures of the Hoveyda–Grubbs second-generation complex (**1**) and its derivatives with a modified phenolic part (**2**–**4'**); (b) interaction mode between the Ru center and the carbonyl oxygen in **4** or **4'**; (c) cross-over reaction of HG-II (**1**) with a ^{13}C-labelled 2-isopropoxybenzilidene ligand.

Motivated by the usability of HG-type complexes, several research groups have developed various HG-type catalysts with

Division of Materials Science, Graduate School of Science and Technology, Nara Institute of Science and Technology (NAIST), Ikoma, Nara 630-0192, Japan. E-mail: tmatsuo@ms.naist.jp

†Electronic Supplementary Information (ESI) available: [Experimental details, crystallographic data, NMR spectral analyses for evaluation of complex stabilities, NMR spectral changes in ligand exchange reactions, crystal structure of HG-II(**1**), IR spectra in the entire measurement range, time-courses and NMR spectral change for metathesis reactions, photographs of reaction solutions, and NMR spectra of synthesized ligands and complexes]. See DOI: 10.1039/x0xx00000x

View Article Online
DOI: 10.1039/D0DT02553A

functionalized ligands for application in syntheses in aqueous media as well as conventional syntheses in organic solvents.[9-11] Furthermore, the applications of HG-type complexes have been extended to the biochemical research field involving chemical modification of biomacromolecules[12, 13] and development of biocatalysts with olefin metathesis activity.[14-16]

One of the well-known strategies for optimizing the catalytic reactivities of HG-type catalysts is through the modification of the phenyl ring in the 2-alkoxybenzylidene ligand. The introduction of electron-withdrawing groups, such as nitro and ammonium groups, into the phenyl ring can directly regulate the coordination of the ether oxygen to the Ru center, accelerating the initial stage of the catalytic cycle.[17,18] In this case, most of the HG-type catalysts have an isopropoxy phenolic part, because the bulkiness of the isopropyl group is believed to appropriately regulate the coordination of the ether oxygen to the Ru center. The above concept is supported by the fact that the replacement of the isopropoxy phenolic part by an adamantyloxy group (**2**), cyclopentoxy group (**3**) or other alkyl/alkoxy groups influences the catalytic activity.[19-21] Furthermore, some HG-type complexes with a phenolic-moiety modified ligand control their catalytic activities by direct interactions between the metal center and a functional group attached to the phenolic moiety (the so-called first-coordination sphere effect).[22, 23] For example, an acetate moiety at the phenolic moiety (**4** and **4'**) weakly coordinates to the Ru center (Fig. 1(b)) to increase the ring-closing metathesis (RCM) activity.[22] In this case, the second interaction of the ester carbonyl oxygen to the metal center in addition to the coordination of the ether oxygen enhances both the stabilities and reactivities of the catalysts. To decrease metal contamination in products, *N*, *O*-dimethylhydroxylamide (Weinreb amide) with high affinity toward silica gel in place of acetate moiety was introduced into the phenolic moiety.[24] As presented above, the structural design for the alkoxy part in the ligand will also increase the divergence in HG-type catalyst derivatives. To evaluate the stabilities and metathesis reactivities of HG-type complexes with the designed ligands, a suitable platform reaction system is required. With this in mind, we focused on a previous finding of the occurrence of a cross-over reaction between ^{13}C-labelled and unlabeled 2-isopropoxybenzylidene ligands in HG-II (**1**) (see Fig. 1(c)).[25] This reaction indicates that a ligand exchange can occur between the 2-isopropoxybenzylidene ligand in HG-II (**1**) and a designed benzylidene ligand. Motivated by this, we established a ligand exchange study between functionalized 2-alkoxybenzylidene compounds and HG-II (**1**) in a 1:1 mixture. Alkoxybenzylidene ligands affording more stable HG-type complexes can be expected to present high conversions in ligand exchange reactions. The relative stabilities of the different complexes were compared to that of HG-II (**1**).

In this study, we built a ligand library composed of 2-alkoxybenzylidene ligands with a modified phenolic part (Scheme 1), to reveal the structural determinants of the stabilities and catalytic activities of HG-II derivatives possessing these ligands. Particularly, we focused on the effects of amide and ester bonds in the terminal phenolic group in 2-alkoxybenzylidene compounds on the efficiencies of the ligand exchange with HG-II (**1**) (**5-amide**–**11-ester**). The selection of amide and ester groups was based on the frequent use of these functional groups as tethering groups to introduce additional building blocks and extend the linker. Based on of our ligand exchange study using several 2-alkoxybenzylidene compounds, we found that the structure composed of a functional group and an ethylene linker at the ligand phenolic part determines the stabilities and reactivities in HG-type complexes through the second-coordination effect. This is a different method to control the properties of HG-type complexes from those reported until now.

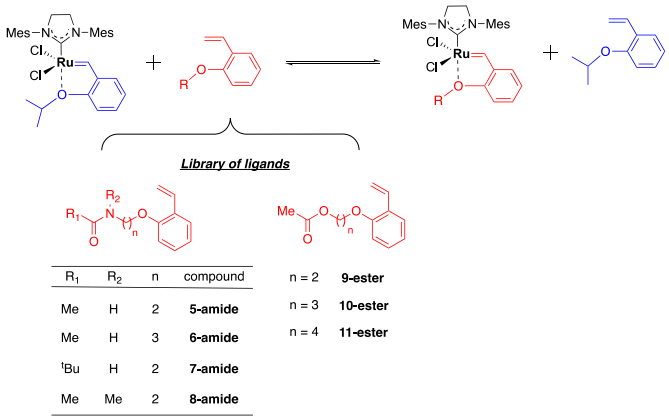

R_1	R_2	n	compound
Me	H	2	**5-amide**
Me	H	3	**6-amide**
^{t}Bu	H	2	**7-amide**
Me	Me	2	**8-amide**

Scheme 1. Ligand exchange between HG-II (**1**) and phenolic part-modified ligands.

Results and discussion

Syntheses of ligands and complexes

The synthetic routes of amide-type ligands (**5-amide**–**8-amide**), ester-type ligands (**9-ester**–**11-ester**), and Ru complexes with these ligands ($[Ru]_{5\text{-amide}}$–$[Ru]_{11\text{-ester}}$) are presented in Schemes 2–4, respectively.

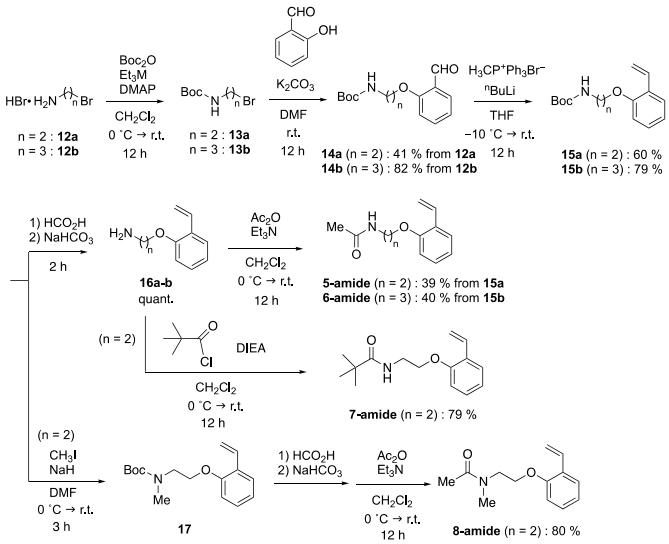

Scheme 2. Synthesis of amide-type ligands.

To obtain the secondary amide ligands (**5-amide**–**7-amide**), the Boc group in compound **15a** or **15b** was deprotected, followed by acylation using acetic anhydride (for **5-amide** and **6-amide**)

View Article Online
DOI: 10.1039/D0DT02353A

or pivaloyl chloride (for **7-amide**). For the synthesis of the *N*-methyl amide ligand (**8-amide**), the nitrogen atom in compound **15a** was methylated under a basic condition, followed by removal of the Boc group. Finally, the secondary amine group was acylated with acetic anhydride to afford compound **8-amide** as a mixture of *cis*/*trans* isomers in the *N*-methyl amide moiety[22] (1:2 ratio at 20 ˚C, see ESI for the NMR spectra).

The ester-type ligands (**9-ester**–**11-ester**) were synthesized from three halogenoalkyl acetate precursors (compounds **19**–**21**). Sequentially, these compounds were subjected to Williamson syntheses and Wittig reactions.

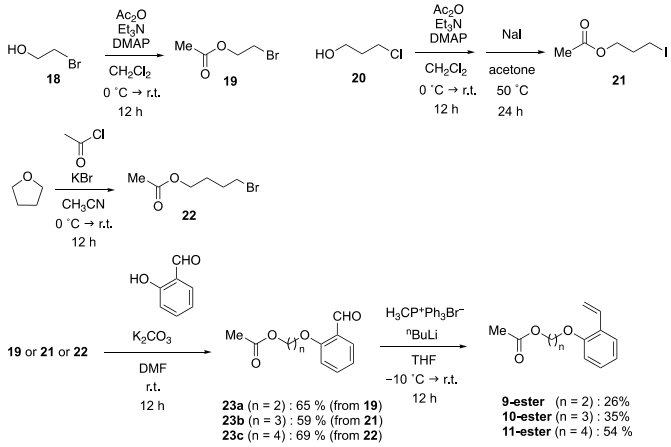

Scheme 3. Synthesis of ester-type ligands.

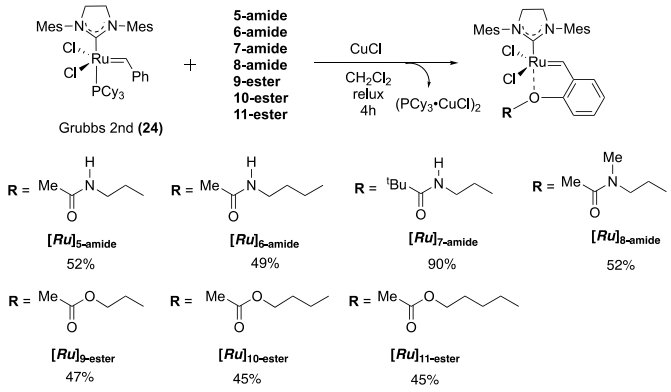

Scheme 4. Synthesis of Ru complexes.

The Ru complexes (**[*Ru*]$_{5\text{-amide}}$**–**[*Ru*]$_{11\text{-ester}}$**) were obtained from the Grubbs second-generation catalyst (**24**) in the presence of CuCl (Scheme 4).[26] All the Ru complexes were isolable as green complexes and stable in air. The moderate yields (45–52%, except for that observed in **[*Ru*]$_{7\text{-amide}}$**) were due to the requirement of removal of unreacted ligands in purification procedures. **[*Ru*]$_{8\text{-amide}}$** was obtained as a mixture of *cis*/*trans* isomers similar to the precursor ligand. The ^{1}H-NMR spectrum of the compound displayed two benzylidene proton peaks at 16.49 ppm and 16.51 ppm (ratio = 2:3; see ESI).

To evaluate the stabilities of these complexes in solutions, we monitored ^{1}H-NMR spectral changes for the complexes in $CDCl_3$ at 25 ˚C over 24 h (Fig. S1–S7) under a N_2 atmosphere. No appearance of new signals nor decrease in signal intensities (with respect to an internal standard) were observed, indicating that the prepared complexes are stable in solutions under the conditions over 24 h.

Ligand exchange reactions between HG-II complex and modified 2-alkoxybenzylidene ligands

Initially, we monitored the ^{1}H-NMR spectral changes caused by the reaction of the HG-II complex (**1**) with ligand **5-amide** to confirm the occurrence of ligand exchange (see Fig. 2 for the magnified spectra and Fig. S8(a) for the entire range of the spectra). For the determination of ligand exchange efficiency, hexamethyldisiloxane (HMDSO, 4 mM) was contained in the reaction solution as an internal standard.

On mixing the HG-II complex and **5-amide** in a 1:1 ratio, the benzylidene proton peak of HG-II (**1**) at 16.560 ppm (peak *a*) gradually decreased along with the appearance of a new peak at 16.640 ppm (peak *A*). We assigned this new peak as the benzylidene proton of the **[*Ru*]$_{5\text{-amide}}$** complex, based on the spectrum of **[*Ru*]$_{5\text{-amide}}$**. The ligand moiety in **[*Ru*]$_{5\text{-amide}}$** was observed (featured by peaks *D*, *E*, and *F*). Another product, free 2-isopropoxybenzylidene ligand (**^{i}Pr-L**), was also detected by the NMR signals at 1.36 ppm (peak *B*) and 4.54 ppm (peak *C*)).

At completion of the reaction after 24 h, we determined the ratio of the two complexes using the intensities of ^{1}H-NMR peaks that are characteristic of each complex (See Fig. S8(b) for relative integration values against HMDSO). From the signal intensities of benzylidene protons (peaks *a* and *A*), the ratio of HG-II(**1**) and **[*Ru*]$_{5\text{-amide}}$** was evaluated to be 18:82. As a double-check, we also determined the complex ratio on the basis of signal intensities of the isopropyl-Me proton in HG-II(**1**) (peak *b*) and acetamide methyl protons at the terminal of ligand in **[*Ru*]$_{5\text{-amide}}$** (peak *D*). A similar value was obtained (20:80). More amount of **[*Ru*]$_{5\text{-amide}}$** than HG-II(**1**) indicates that **[*Ru*]$_{5\text{-amide}}$** is more stable than HG-II(**1**). Some peaks with small intensities near peaks *B* and *D* (peaks with asterisks in Fig. 2(c)) may derive from the cross-metathesis products. A tiny signal at 5.4 ppm (ethylene protons[27]) was also observed at 24 h. From the calculated total amount of the two complexes (40–42 mM), the percentage of metathesis products was estimated to be <5%; namely, the observed spectral change is mainly associated with the conversion from HG-II(**1**) into **[*Ru*]$_{5\text{-amide}}$**. On the addition of excess **^{i}Pr-L** (20 eq.) to the reaction mixture after 24 h, the intensity of peak *A* tended to decrease, in turn, peak *a* relatively increased over the further 24 h (Fig. S9). During this period, the isopropyl-CH proton in HG-II(**1**) (peak *c*) and free **5-amide** (featured by peaks *d* and *e*) recovered. The spectral change displayed the back reaction from **[*Ru*]$_{5\text{-amide}}$** to HG-II(**1**), indicating that the spectral changes shown above reflects a reversible process (i.e. equilibrium).

Next, we examined other 2-alkoxybenzylidene ligands for a ligand exchange study to reveal the effects of the functional groups in these ligands on the efficiency of the ligand exchange reaction. Table 1 summarizes the ratio of HG-II(**1**) and complexes produced by ligand exchange at 24 h. The time-courses of the ratios of HG-II(**1**) between the complexes produced by the ligand exchange) are illustrated in Fig. 3 (see spectral changes in Figs. S10–S15).

View Article Online
DOI: 10.1039/D0DT02353A

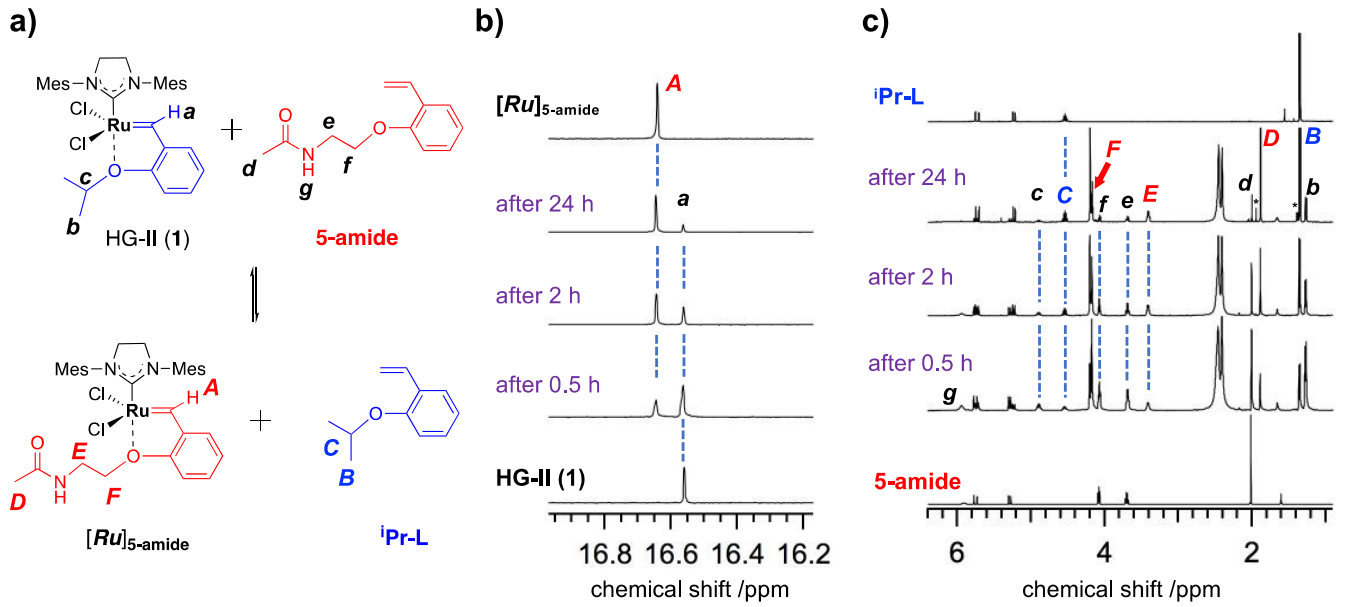

Fig. 2. Ligand exchange between HG-II (**1**) and ligand **5-amide** ([HG-II (**1**)] = [**5-amide**] = 42 mM in $CDCl_3$, 25 °C under N_2). (a) Reaction scheme, (b) 400-MHz ^{1}H-NMR spectral change (downfield region), and (c) 400-MHz ^{1}H-NMR spectral change (upfield region). The spectral changes in the entire region are presented in Fig. S8(a). The spectra of HG-II (**1**), **[*Ru*]$_{5\text{-amide}}$**, **^{i}Pr-L**, and **5-amide** were collected separately as authentic samples for the comparison of the chemical shift. The signals with an asterisk (*) are ascribed to cross-metathesis products (< 5%).

Table 1. Ratio of HG-II(**1**) and complexes produced by ligand exchange (HG-II(**1**) : product complex at 24 h)[a,b]

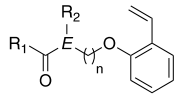

E = N (amide-type liagnds) or O (ester-type ligands)

Ligand	n	R_1	R_2	Ratio value	
				determined from benzylidene protons	determined from ^{i}Pr-Me protons in HG-II(**1**) and Me (or ^{t}Bu) protons in product complex[c]
5-amide	2	Me	H	18 : 82	20 : 80
6-amide	3	Me	H	39 : 61	38 : 62[d]
7-amide	2	^{t}Bu	H	n.d.[e]	23 : 77
8-amide	2	Me	Me	69 : 31	69 : 31
9-ester	2	Me	H	n.d[e]	81 : 19
10-ester	3	Me	H	n.d[e]	59 : 41
11-ester	4	Me	H	52 : 48	49 : 51

[a][HG-II(**1**)]/[ligand] = 1/1 (42 mM) in $CDCl_3$ (sealed in a J-young NMR tube) at 25 ˚C under an N_2 atmosphere in the presence of an internal standard (hexamethyldisiloxane (HMDSO, 4 mM). [b]Determined from the relative integration values based on the peak intensity of HMDSO (0.066 ppm). [c] To determine the amount of product complexes, the peak intensities of methyl or ^{t}Bu protons at the terminal of a ligand in product complexes were employed. [d]The peak of terminal Me protons overlaps with that of methylene linker; Thereby, the peak intensity was calculated as five protons (3H+2H). [e]Not determined due to overlap of signals in HG-II(**1**) and product complexes.

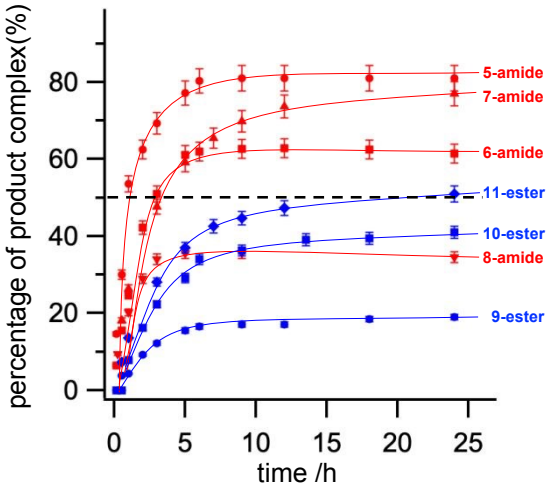

Fig. 3. Time-courses of the complex ratio (HG-II (**1**) : complex produced by ligand exchange); red: amide ligands; blue: ester ligands. Errors bars are drawn at 4%. Reaction conditions: [HG-II (**1**)]/[ligand] = 1/1 (42 mM) in $CDCl_3$ (sealed in a J-young NMR tube) at 25 °C under a N_2 atmosphere in the presence of HDMSO (internal standard, 4 mM).

In the reactions with the secondary amide-type ligands (*i.e.*, RC(=O)NH-), **5-amide**, **6-amide**, and **7-amide**, the percentages of the complexes with these ligands among all the complexes in the reaction system (corresponding to the ligand exchange conversion) exceeded 50%. In contrast, all the ester ligands had comparatively lower ratios. The final ratios of the formed complexes reflect their relative stabilities compared to HG-II (**1**): the ratio of >50% indicate that these complexes produced by the ligand exchange reactions are more stable than HG-II (**1**). The above finding indicates that a secondary amide group in the phenolic moiety in HG-type ligands is essential for stabilizing

their complexes, whereas an ester group will reduce their stabilities. Focusing on the effects of the linker length (*i.e.*, the distance between the phenolic oxygen atom and the amide (or ester) group) on the ligand exchange, we found that **5-amide** (n = 2) presented the *highest* ligand exchange efficiency among the ligands tested in this study; in contrast, **9-ester** (n = 2) resulted in the *lowest* conversion. Thus, $[Ru]_{\text{5-amide}}$ and $[Ru]_{\text{9-ester}}$ are the most and least stable complexes, respectively, among the complexes produced by ligand exchange reactions although the respective linkers have the same length (n = 2). Another finding was that the ligand exchange conversions tended to be closer to 50% with long linker lengths (conversions at the final state: **5-amide** (n = 2) ~ **7-amide** (n = 2) > **6-amide** (n = 3) |50%| **11-ester** (n = 4) > **10-ester** (n = 3) > **9-ester** (n = 2)). Concurrently, the effect of the amide (or ester) group on the ligand exchange efficiency diminished. Specifically, the length of the ethylene linker (n = 2) is a structural factor for reflecting the functional group effect on the ligand exchange efficiency. Although their linker lengths are identical (n = 2), **5-amide** achieved a more rapid ligand exchange than **7-amide**, which is attributed to the steric hindrance caused by the terminal function group in these ligands (Me versus ^{t}Bu group).

As an exception among the amide ligands, **8-amide**, a tertiary amide ligand (*N*-methyl amide), displayed a low ligand exchange efficiency (~30%). Based on this finding, we assumed that an amide proton (N–*H*) is essential for stabilizing the complexes. An amide proton may form a hydrogen bond to interact with another part in the complex, where the ethylene linker (n = 2) has the ideal length for interacting effectively with an amide proton. The corresponding structural investigation is described in detail subsequently.

X-ray crystallographic analysis: Structural effect of amide group on complex stability

To clarify the effects of an ethylene amide/ester moiety on ligand exchange efficiency (i.e. the stabilities of the above-mentioned complexes) we, firstly, conducted single crystal structural analyses for $[Ru]_{\text{5-amide}}$ (n = 2; amide), $[Ru]_{\text{9-ester}}$ (n = 2; ester), $[Ru]_{\text{6-amide}}$ (n = 3; amide), and $[Ru]_{\text{10-ester}}$ (n = 3; ester), (Fig. 4). Detailed crystallographic parameters and structure refinements are summarized in Table S1. For structural comparison, we also analyzed the structure of HG-II (**1**) under the same crystallization solvent system and diffraction collection temperature as those used for the crystallization of the above-mentioned four complexes (Fig. S16 and Table S1). Selected structural information (distances between the Ru center and the atoms coordinating to it and the dihedral angles along C(8)–C(9) axis) is provided in Table 2.

The overall coordination geometries around the metal centers in the four Ru complexes are similar to that in HG-II (**1**) (see the Ru(1)–C(1) and Ru(1)–carbene carbon distances). Against HG-II(**1**), $[Ru]_{\text{5-amide}}$ and $[Ru]_{\text{9-ester}}$ have the opposite relative stabilities. However, these two complexes have similar Ru(1)–O(1) distances (see Table 3) with the larger distance observed in HG-II (**1**). The similar bond distances in these complexes are not unusual because several previous works reported that the Ru(1)–O(1) strengths do not always correlate with the Ru(1)–O(1) bond distances among HG-type complexes.[19-21] However, in $[Ru]_{\text{5-amide}}$ and $[Ru]_{\text{10-ester}}$ (*i.e.*, complexes with an n = 3 linker), the Ru(1)–O(1) distances tend to be close to that in HG-II (**1**). The observed tendency indicates that the long Ru(1)–O(1) bonds in $[Ru]_{\text{5-amide}}$ and $[Ru]_{\text{9-ester}}$ (n = 2) may be caused by any structural factors at other places than their metal coordination site (for example, the amide or ester moiety in the ethylene linker part). The dihedral angles of O(1)–C(8)–C(9)–N(1) (or O(2)) of $[Ru]_{\text{5-amide}}$ and $[Ru]_{\text{9-ester}}$ are –64.38° and +77.95°, respectively, with typical synclinal conformations (Figs 4(a) and 4(b)). The long linker length in $[Ru]_{\text{6-amide}}$ and $[Ru]_{\text{10-ester}}$ results in the increase in the dihedral angles. Particularly, $[Ru]_{\text{10-ester}}$ displays an anti-periplanar conformation, an ideally relaxed conformation.

Table 2. Selected structural information of Ru Complex crystals[a]

Ru complex	Ru(1)-O(1) distance /Å	Ru(1)-C(1) distance /Å	Ru(1)-carbene carbon distance /Å	Dihedral angle along C(8)–C(9)[b]
$[Ru]_{\text{5-amide}}$ (n = 2)	2.278(1)	1.830(2)	1.978(2)	–64.4(2)° (O(1)–C(8)–C(9)–N(1))
$[Ru]_{\text{9-ester}}$ (n = 2)	2.277(1)	1.831(2)	1.978(2)	+77.9(2)° (O(1)–C(8)–C(9)–O(2))
$[Ru]_{\text{6-amide}}$ (n = 3)	2.256(2)	1.832(2)	1.976(3)	+70.0(3)° (O(1)–C(8)–C(9)–C(10))
$[Ru]_{\text{10-ester}}$ (n = 3)	2.245(2)	1.830(2)	1.981(2)	+179.5(2)° (O(1)–C(8)–C(9)–C(10))
HG-II(**1**)	2.233(2) 2.261(3)[c]	1.832(2) 1.828(5)[c]	1.975(2) 1.981(5)[c]	–

[a]Crystals were obtained by vapor diffusion of hexane into a $CHCl_3$ solution at 5 °C. X-ray diffraction was collected at 125 ± 0.1 K. [b]Sign (+ or –) was defined along the axis direction from C8 to C9, where "+" and "–" were defined in the counter clockwise and clockwise directions, respectively. [c]Ref.26; Diffraction was collected at 273 K.

Focusing on the amide moiety in $[Ru]_{\text{5-amide}}$ (see Fig. 4(b)), we found that the spatial distance between N(1) and Cl(1) is 3.233 Å, corresponding to the sum of the van der Waals radii of nitrogen and chlorine atoms (N: 1.50 Å; Cl: 1.75 Å). The small distance between the two atoms indicates the occurrence of any interaction between these atoms. On the basis of the geometry around N(1) atom, the amide hydrogen (N–*H*) is assumed to turn to Cl(1) (not exactly determined by the X-ray crystallography). Therefore, one possible interaction occurred at this site is the N–H•••Cl hydrogen bonding. Several reports have presented the stabilization of metal complexes through intramolecular N–H•••Cl hydrogen bonding,[28, 29] where N–Cl distances are 3.1–3.4 Å and estimated N–H–Cl angles are in the range from 135° to 170°. The estimated N–H–C angle of $[Ru]_{\text{5-amide}}$ (150.96°) is within this range (see magnified figure around the amide moiety in $[Ru]_{\text{5-amide}}$ in Fig. S17).

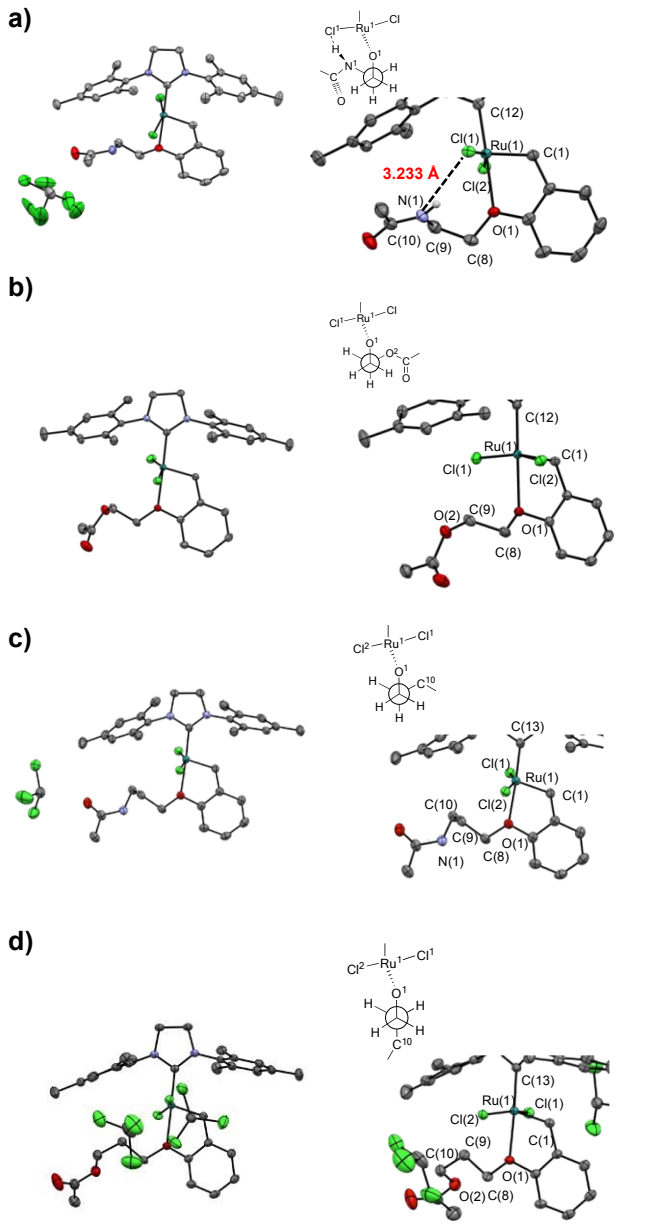

Fig. 4. ORTEP figures of (a) **[*Ru*]$_{5\text{-amide}}$**, (b) **[*Ru*]$_{9\text{-ester}}$**, (c) **[*Ru*]$_{6\text{-amide}}$**, and (d) **[*Ru*]$_{10\text{-ester}}$**. The structures on the right of each figure show the local structures around the Ru centers. Thermal ellipsoids are drawn at 50% probability level. In the magnified structure of figure (a), the amide hydrogen was assumed according to the geometry around atom N(1).

Another possibility of an interaction at the amide moiety is N–Cl halogen bonding (denoted as XB).[30] In general, XB is classified into two types according to geometries of an XB donor and acceptor; type-I (*cis*/*trans*) and type-II.[31] Assuming the occurrence of XB at this site, we can raise two possibilities of XB on the basis of the local geometry around the site: *cis*-type-I XB (Ru(1)–Cl(1)•••N(1)–C(9)) and *trans*-type-I XB (Ru(1)–Cl(1)•••N(1)–C(10)). The Ru(1)–Cl(1)–N(1) dihedral angle (= θ_1) is 79.83°. The Cl(1)–N(1)–C(9) and Cl(1)–N(1)–C(10) dihedral angles (defined as θ_2 and θ_2', respectively) are 109.31° and 124.59°, respectively (see Fig. S17). Namely, $|\theta_1-\theta_2| = 29.5°$ and $|\theta_1-\theta_2'| = 44.8°$. According to several examples of XBs,[32] most of type-I XB units have $|\theta_1-\theta_2|$ values of $\leq$ 20°. The calculated values of $|\theta_1-\theta_2|$ and $|\theta_1-\theta_2'|$ for **[*Ru*]$_{5\text{-amide}}$** are too large as a type-I XB geometry. Furthermore, if XB occurred between Cl(1) and N(1), **8-amide** with an *N*-Me amide moiety (more electron-donating characteristic) would also form XB with Cl(1). However, the ligand exchange data (Table 1 and Fig. 3) presented above do not indicate the interaction with Cl(1) atom. The possibility of Cl(1)•••N(1) XB cannot be completely ruled out; however, the N–H•••Cl hydrogen is more likely as an interaction between the amide moiety in **[*Ru*]$_{5\text{-amide}}$**. The interaction may cause the amide nitrogen to adopt a position with a small O(1)–C(8)–C(9)–N(1) dihedral angle (close to the Gauche form).

In contrast, the ester oxygen atom (O(2)) in **[*Ru*]$_{9\text{-ester}}$** was found to turn away from the direction of Cl(1) so as to avoid the electrostatic repulsion with the chlorido ligand. The synclinal conformation observed in **[*Ru*]$_{9\text{-ester}}$** is a result of the avoidance of the steric hindrance between the ester carbonyl group and the NHC phenyl ring in the periplanar conformation.

Investigation of N–H ••• Cl hydrogen bonding in solution

To confirm that N–H•••Cl hydrogen in **[*Ru*]$_{5\text{-amide}}$** also occurs in solutions (*i.e.*, it is not caused by the crystal packing factor), we investigated the N–H/D exchange velocity in **5-amide** and **[*Ru*]$_{5\text{-amide}}$** by ^{1}H-NMR spectral monitoring. The NMR spectral changes in the presence of D_2O are depicted in Fig. 5.

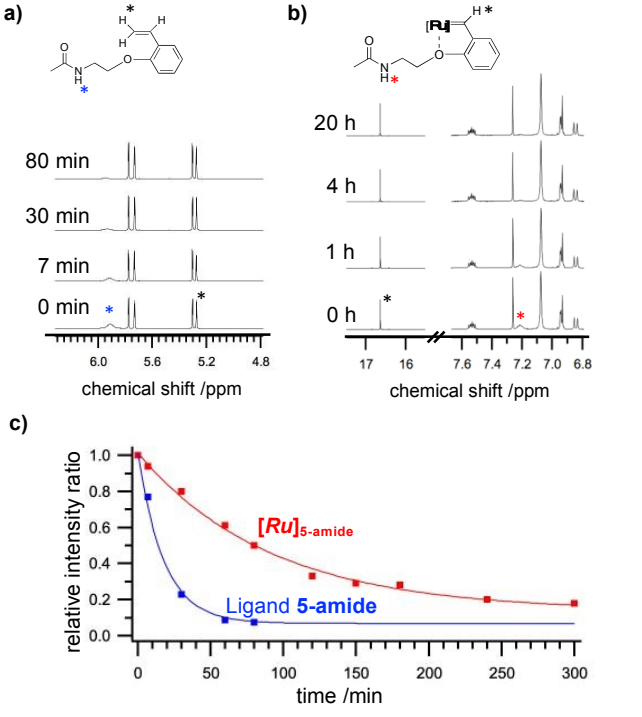

Fig. 5. 400-MHz ^{1}H-NMR spectral changes (in $CDCl_3$, 600 μL) involving the H/D exchange on the addition of D_2O (1% (v/v)) at 25 °C under N_2 atmospheres: (a) ligand **5-amide** (0.02 M) and (b) complex **[*Ru*]$_{5\text{-amide}}$** (0.02 M). (c) Time-courses of the relative intensities of the N–H proton signals (marked in red or blue asterisk in (a) and (b)) to the peak intensities of an unexchangeable proton (marked in black asterisk in (a) and (b)).

The amide proton peaks in **5-amide** and **[*Ru*]$_{5\text{-amide}}$** appear at 5.78 ppm and 7.21 ppm, respectively. The above comparatively

higher chemical shifts observed for $[Ru]_{5\text{-amide}}$ suggest that its amide proton participates in a strong hydrogen bonding. The time-courses of the H/D exchange reactions were monitored using the peak intensity ratio of the amide proton in each compound and a non-exchangeable proton (an olefin proton in **5-amide** observed at 5.26 ppm; the benzylidene proton in $[Ru]_{5\text{-amide}}$ at 16.64 ppm). The half-time values of the H/D exchange observed for **5-amide** and $[Ru]_{5\text{-amide}}$ are 12 min and 63 min, respectively. The deaccelerated N–H/D exchange in $[Ru]_{5\text{-amide}}$ is indicative of a hydrogen bonding involving the amide proton.

The chemical shifts of the amide protons in the amide-type Ru complexes are ranked as $[Ru]_{5\text{-amide}}$ (7.21 ppm) > $[Ru]_{8\text{-amide}}$ (7.12 ppm) > $[Ru]_{7\text{-amide}}$ (6.53 ppm), consistent with the order of the ligand exchange efficiency. In addition, this finding proves that the N–H••• Cl hydrogen bonding also occurs in solution.

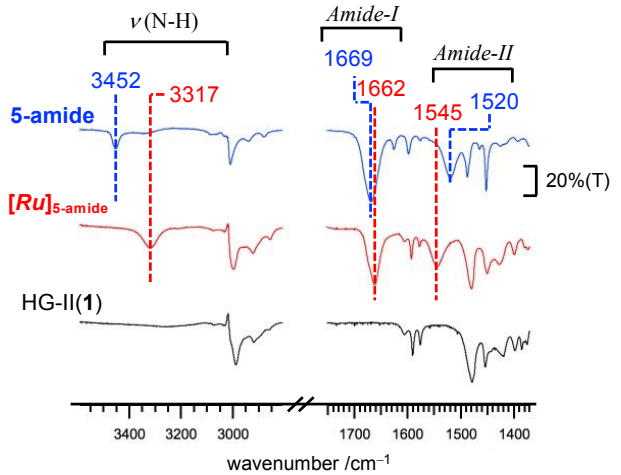

Fig. 6. FT-IR spectra of **5-amide**, $[Ru]_{5\text{-amide}}$, and HG-II (**1**) in $CHCl_3$ (resolution of 0.5 cm^{-1}, L = 0.5 mm, CaF_2 window, accumulation number: 256). Each spectrum is obtained by subtracting the background spectrum of chloroform from the corresponding collected spectrum of the ligand or complex.

We also investigated the N–H•••Cl hydrogen bonding in terms of the bond characteristics of the amide moiety via Fourier transform infrared (FT-IR) spectroscopy. Fig. 6 depicts the FT-IR spectra of **5-amide**, $[Ru]_{5\text{-amide}}$, and HG-II (**1**) (see the spectra over the entire measurement range in Fig. S18). In the low-wavenumber range, the bands at 1660–1670 cm^{-1} and 1520–1550 cm^{-1} observed in **5-amide** and $[Ru]_{5\text{-amide}}$ are assigned as amide-I (ν(C=O)) and amide-II (coupling of ν(C–N) and δ(N–H)), respectively. This assignment is confirmable by comparing their spectra to that of HG-II (**1**) (without an amide bond in the structure). Complex $[Ru]_{5\text{-amide}}$ presents a decrease in frequency of the C=O vibration with an increase in the frequency of the C–N vibration coupled with N–H bending. This indicates that the N–H•••Cl hydrogen bonding enhances the contribution of the C=N bonding character in the amide bond. The perturbation of the N–H bonding is remarkably reflected in the high-wavenumber region, where the amide N–H stretching (ν(N–H)) of $[Ru]_{5\text{-amide}}$ appears at 3317 cm^{-1}, whereas the ν(N–H) of ligand **5-amide** is 3452 cm^{-1}. The complete red-shift of ν(N-H) observed in $[Ru]_{5\text{-amide}}$ suggests that there is significant N–H•••Cl hydrogen bonding in the solution structure. The series of crystallographic investigation, H/D exchange kinetics, and amide vibration analyses presented above prove that the N–H•••Cl hydrogen bonding occurs both in the crystal and solution states. The N–H•••Cl hydrogen bonding in $[Ru]_{5\text{-amide}}$ contributes to complex stabilization. The stabilization effect decreases with increase in the linker length. The electrostatic repulsion in $[Ru]_{9\text{-ester}}$ is a main factor that the decrease in the relative stability of this complex toward HG-II(**1**). The enhancement of the ligand exchange efficiency with increasing linker length in the series of ester-type Ru complexes is attributed to the diminishment of this electrostatic repulsion between the ester oxygen and the chlorido ligand that coordinates to the Ru center.

Effects of ethylene amide/ester moiety in ligand on catalytic activities.

Complexes $[Ru]_{5\text{-amide}}$ and $[Ru]_{9\text{-ester}}$ commonly have an ethylene linker at their benzylidene ligand moieties and exhibit similar Ru-O distances. However, the complexes showed a distinctly opposite tendency in the relative stability against HG-II(**1**), which is caused by the structural factors that are seen apart from the Ru center. In this view, our next concerns will be the effects of these structural factors on their catalytic activities. Accordingly, we conducted some metathesis reactions to compare the reactivities of these complexes with that of HG-II(**1**) to explore effects of the amide or ester group in $[Ru]_{5\text{-amide}}$ (the most stable complex) and $[Ru]_{9\text{-ester}}$ (the least stable complex) on their catalytic activities, (Table 3).

We, at first, carried out the ring-closing metathesis (RCM) of compound **25** to coumarin **26** at 5 mol% catalyst loading because the moderate rate of this reaction enables us to readily conduct the comparison of the reactivities between the complexes.[33] The time-courses of the RCM products and the NMR spectral changes observed in the $[Ru]_{5\text{-amide}}$-catalyzed reaction are displayed in Fig. S19, as a representative example of the monitored RCM reactions. All the three Ru complexes exhibited the RCM cyclization activity for compound **25** with final yields of >94% at 5 mol% catalyst load (Entries 1–3 in Table 3). The reaction velocities follow the order, $[Ru]_{9\text{-ester}}$ > HG-II(**1**) > $[Ru]_{5\text{-amide}}$.

The slower velocity in the $[Ru]_{5\text{-amide}}$-mediated reaction, compared to other two catalysts, was also observed in the reaction of *N*-tosyldiallylamide **27** (Entries 4–6 in Table 2). One possible reason of the slow $[Ru]_{5\text{-amide}}$-catalyzed reactions is that the N–H•••Cl hydrogen bonding in $[Ru]_{5\text{-amide}}$ deaccelerates the exchange between the 2-alkoxybenzilidene ligand and a substrate molecule. However, the existence of several pathways at the initiation step in HG-type catalyst-mediated reactions has been known (denoted as dissociative and associative/interchange pathways).[34-36] The contribution of these pathways depends on substrate concentrations (i.e. the relative ratio of catalyst to substrate). To investigate this matter, we conducted the RCM reaction at low catalyst load (0.1 mol%; Entries 7–9 in Table 3; see the time-courses of the $[Ru]_{5\text{-amide}}$-catalyzed reaction in Fig. S20). All the complexes showed the final yields of >90%. The order of reaction velocity (evaluated by the yield the initial phase) was $[Ru]_{9\text{-ester}}$ > HG-II(**1**) > $[Ru]_{5\text{-amide}}$, which is the same

View Article Online
DOI: 10.1039/D0DT02353A

tendency as that seen in the reaction of compound **25** with 5 mol% catalyst load (Entries 1–3 in Table 3).

Table 3. RCM activities of $[Ru]_{5\text{-amide}}$, $[Ru]_{9\text{-ester}}$, and HG-II(**1**)[a,b]

Entry	Substrate	Product	Catalyst	Reaction conditions	Yield(%)[c]
1	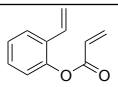 **25**	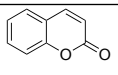 **26**	$[Ru]_{5\text{-amide}}$	5 mol%; 25 ˚C	15 (2 h); 94 (54 h)
2			$[Ru]_{9\text{-ester}}$	5 mol%; 25 ˚C	83 (2h); 95 (24 h)
3			HG-II(**1**)	5 mol%; 25 ˚C	53 (2 h); 99 (24 h)
4	 **27**	 **28**	$[Ru]_{5\text{-amide}}$	5 mol%; 25 ˚C	30 (0.5 h); >99 (7 h)[d]
5			$[Ru]_{9\text{-ester}}$	5 mol%; 25 ˚C	>99 (0.5 h)[d]
6			HG-II(**1**)	5 mol%; 25 ˚C	>99 (0.5 h)[d]
7			$[Ru]_{5\text{-amide}}$	0.1 mol%; 25 ˚C	11 (0.5 h); 91 (24 h)
8			$[Ru]_{9\text{-ester}}$	0.1 mol%; 25 ˚C	85 (0.5 h); >99 (24 h)[d]
9			HG-II(**1**)	0.1 mol%; 25 ˚C	63 (0.5 h); >99 (24 h)[d]
10			$[Ru]_{5\text{-amide}}$	5 mol%; 45 ˚C	>99 (0.5 h)[d]
11			$[Ru]_{9\text{-ester}}$	5 mol%; 45 ˚C	>99 (0.5 h)[d]
12			HG-II(**1**)	5 mol%; 45 ˚C	>99 (0.5 h)[d]
13	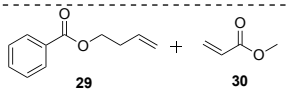 **29** + **30** (**29** : **30** = 1 : 2)	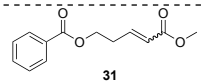 **31**	$[Ru]_{5\text{-amide}}$	1 mol%; 25 ˚C	**31**[e]: 19 (2 h); 37 (24 h) **32**[e]: < 5 (2 h); 5 (24 h)
14			$[Ru]_{9\text{-ester}}$	1 mol%; 25 ˚C	**31**[e]: 54 (2 h); 61 (24 h) **32**[e]: 7 (2 h); 8 (24 h)
15		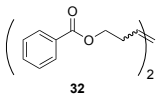 **32**	HG-II(**1**)	1 mol%; 25 ˚C	**31**[e]: 48 (2 h); 74 (24 h) **32**[e]: 5 (24 h); 6 (24 h)

[a][substrate] = 42 mM in $CDCl_3$ in the dark at a N_2 atmosphere. [b]Reaction was conducted in a J-young tube (Entries 1–10) or in a Schlenk tube (Entries 11–12). [c]Determined by ^1H NMR measurements for a reaction mixture that contains an internal standard (Entries 1–3 and 13–15: HMDSO (4 mM, δ_H 0.066 ppm), Entries 4–12: toluene (42 mM, δ_H 2.356 ppm)). [d]Starting material cannot be precisely quantified because of tiny peaks on ^1H NMR spectra. [e]*E*/*Z* > 20/1.

Considering the intrinsically higher stability of $[Ru]_{5\text{-amide}}$ than the other two complexes, the most possible mechanism to explain the results of catalytic activity measurements is that the slow velocities of $[Ru]_{5\text{-amide}}$-mediated reactions are predominantly caused by the slow dissociation of the benzylidene ligand in $[Ru]_{5\text{-amide}}$ at the initial phase. The slow initiation of catalytic reaction is led by the interaction between the amide moiety and a chloride ligand. The interaction will decrease at higher temperatures. In fact, $[Ru]_{5\text{-amide}}$ also showed a comparable reactivity to the other two complexes at 45 ˚C, where the reaction completed at 0.5 h (*cf.* Entries 4 and 10). At the temperature, the exchange of the benzylidene ligand with a substrate molecule can be facilitated. On the other hand, $[Ru]_{9\text{-ester}}$ showed the faster initial velocities than HG-II(**1**) in all cases of RCM reactions (*cf.* Entries 2 and 3; Entries 8 and 9; Figs. S19 and S20). As described above, the ester oxygen atom (O(2)) adopts the positioning to turn away from the metal center (see Fig. 4(d)). The acceleration observed in $[Ru]_{9\text{-ester}}$ may also be explained by the electrostatic repulsion between the oxygen atom and a chlorido ligand. The conformation will promote the dissociation of the benzylidene ligand moiety, leading to the facilitation of initial phase in catalytic reactions.

The slow initial reaction for $[Ru]_{5\text{-amide}}$ was also observed in cross-metathesis (CM) reaction between compound **29** and **30** (Entries 13–15). In the $[Ru]_{9\text{-ester}}$-catalyed CM reaction, the initial CM production (compounds **31**/**32**) was higher than that mediated by HG-II(**1**). However, we observed that the change in solution color (green to brown) was significant compared to the reactions mediated by the other two complexes. Eventually, the product yield in the $[Ru]_{9\text{-ester}}$-catalyed reaction was lower than that mediated by HG-II(**1**) reaction.

At first glance, $[Ru]_{5\text{-amide}}$ seems to have a drawback in terms of the reaction velocity. However, during the reaction of compound of **27** at 45 ˚C, we found that the reaction mixture with $[Ru]_{5\text{-amide}}$ after the complete of the reaction still kept green in color (a characteristic in HG-type complexes), whereas the solution with $[Ru]_{9\text{-ester}}$ had turned to brown (indicative of degradation) (Fig. S22). The relative stability of $[Ru]_{5\text{-amide}}$ at room temperature is higher than HG-II(**1**). Although we need to investigate in detail, our finding regarding the color change would suggest the potential of $[Ru]_{5\text{-amide}}$ as a durable catalyst that can be thermally activated.

Regulation of HG-type complex properties through second-coordination sphere effects

Previous studies on HG-type complex-mediated olefin metathesis reactions have mainly focused on the coordination properties at the Ru center to discuss the reactivities of the complexes. However, the stability and catalytic activities of $[Ru]_{5\text{-amide}}$ and $[Ru]_{9\text{-ester}}$ are determined by the interactions at rather far from the reaction site, which is a different mechanism from that reported in previous studies.

The N–H•••Cl hydrogen bonding in $[Ru]_{5\text{-amide}}$ and the electronic repulsion between the ester moiety and a chlorido ligand in $[Ru]_{9\text{-ester}}$ affect the stabilities and reactivities of these complexes, where these structural factors indirectly influence the

reactivities of their Ru centers. The structural effect is known as "second-coordination sphere effect", and the above-presented findings indicate that the properties of metathesis catalysts can be affected by second-coordination sphere effects as well as the characteristics of ligands that directly coordinates to the mental center. The attachment of a functional group to the phenolic moieties in HG-type complexes enables tuning its effects on their metal center reactivities, with the linker length between the phenolic oxygen atom and the introduced functional group being crucial. The importance of the linker length emerged as a mechanistic difference between $[Ru]_{5\text{-amide}}$/$[Ru]_{9\text{-ester}}$ and compounds **4**/**4'** (comparison of the structural influences displayed in Figs. 1(b) and 4). Thus, a change in the linker length may switch the mechanism for controlling the reactivities of HG-type complexes (*i.e.*, between first- and second-coordination sphere effects).

Conclusion

In Hoveyda-Grubbs-type complexes with a modified 2-alkoxybenzylidene ligand, a functional group attached to the terminal of phenolic moiety in the ligand may influence the reactivities of the complexes, without any perturbation to the manner of coordination around the metal center. This fact is a noticeable issue in the design of functionalized Hoveyda-Grubbs-type complexes in addition to the structural modulation for the metal coordination site, a traditionally adopted strategy.

In this study, the ligand exchange reaction between the HG-II complex and a designed 2-alkoxybenzylidene ligand was found to be useful for evaluating the stability of the complex with the designed ligand. The existence of an amide or ester group in the ethylene linker extending from the phenolic oxygen influences the stabilities and metathesis activities of the complexes. It was revealed that the interaction between the functional group attached to the phenolic moiety and a chlorido ligand is able to work as a determinant of the complex properties, where no perturbation to the manner of coordination around the metal center occurred. The single-crystal X-ray and solution NMR/IR spectroscopic analyses proved that the indirect effects on the metal center are due to structural factors at the outer sphere (i.e. second-coordination sphere effects). The catalytic activities were also influenced by the functional group at the terminal of the phenolic moiety in the ligand. Therefore, in functionalization of metathesis-mediating catalysts, second-coordination sphere effects should be taken into consideration as one important factor to determine the reactivities of catalysts, along with traditionally discussed factors such as the coordination fashion to the metal center.

Conflicts of interest

There are no conflicts to declare.

Acknowledgements

This work was supported by a Grant-in Aid for Scientific Research on Innovative Areas "Molecular Engine" (JSPS KAKENHI Grant Number JP19H05395) and a Grant-in-Aid for Scientific Research (C) (JSPS KAKENHI Grant Number JP17K01947). C. J. acknowledge Faculty of Pharmacy, University of Indonesia for granting permission to him to study in NAIST, Japan. The authors acknowledge Yoshiko Nishikawa for support of mass analyses and Shohei Katao for X-ray crystallographic analyses.

Notes and references

1. D. Hughes, P. Wheeler and D. Ene, *Org. Process Res. Dev.*, 2017, **21**, 1938-1962.
2. C. Lecourt, S. Dhambri, L. Allievi, Y. Sanogo, N. Zeghbib, R. Ben Othman, M. I. Lannou, G. Sorin and J. Ardisson, *Nat. Prod. Rep.*, 2018, **35**, 105-124.
3. O. M. Ogba, N. C. Warner, D. J. O'Leary and R. H. Grubbs, *Chem. Soc. Rev.*, 2018, **47**, 4510-4544.
4. B. M. Trost, M. Machacek and M. J. Schnaderbeck, *Org. Lett.* 2000, **2**, 1761-1764.
5. L. Wu, I. Fleischer, R. Jackstell and M. Beller, *J. Am. Chem. Soc.*, 2013, **135**, 3989-3996.
6. K. M. Kuhn, J.-B. Bourg, C. K. Chung, S. C. Virgil and R. H. Grubbs, *J. Am. Chem. Soc.* 2009, **131**, 5313-5320.
7. V. Paradiso, V. Bertolasi, C. Costabile, T. Caruso, M. Dąbrowski, K. Grela and F. Grisi, *Organometallics*, 2017, **36**, 3692-3708.
8. A. Perfetto, V. Bertolasi, C. Costabile, V. Paradiso, T. Caruso, P. Longo and F. Grisi, *RSC Advances*, 2016, **6**, 95793-95804.
9. K. Skowerski, G. Szczepaniak, C. Wierzbicka, Ł. Gułajski, M. Bieniek and K. Grela, *Catal. Sci. Technol.*, 2012, **2**.
10. A. Sytniczuk, A. Kajetanowicz and K. Grela, *Catal. Sci. Technol.*, 2017, **7**, 1284-1296.
11. B. J. J. Timmer, O. Kravchenko and O. Ramström, *ChemistrySelect*, 2020, **5**, 7254-7257.
12. B. Bhushan, Y. A. Lin, M. Bak, A. Phanumartwiwath, N. Yang, M. K. Bilyard, T. Tanaka, K. L. Hudson, L. Lercher, M. Stegmann, S. Mohammed and B. G. Davis, *J. Am. Chem. Soc.*, 2018, **140**, 14599-14603.
13. Y. A. Lin, J. M. Chalker and B. G. Davis, *ChemBioChem*, 2009, **10**, 959-969.
14. H. J. Davis and T. R. Ward, *ACS Cent. Sci.*, 2019, **5**, 1120-1136.
15. T. Matsuo, T. Miyake and S. Hirota, *Tetrahedron Lett.*, 2019, **60**, 151226(1)-121226(8).
16. D. F. Sauer, S. Gotzen and J. Okuda, *Org. Biomol. Chem.*, 2016, **14**, 9174-9183.
17. A. Michrowska, R. Bujok, S. Harutyunyan, V. Sashuk, G. Dolgonos and K. Grela, *J. Am. Chem. Soc.*, 2004, **126**, 9318-9325.
18. A. Michrowska, Ł. Gułajski, Z. Kaczmarska, K. Mennecke, A. Kirschning and K. Grela, *Green Chem.* 2006, **8**, 685-688.
19. K. M. Engle, G. Lu, S. X. Luo, L. M. Henling, M. K. Takase, P. Liu, K. N. Houk and R. H. Grubbs, *J. Am. Chem. Soc.*, 2015, **137**, 5782-5792.
20. A. Zieliński, G. Szczepaniak, R. Gajda, W. K., B. Trzaskowski, D. Vidović, A. Kajetanowicz and K. Grela, *Eur. J. Inorg. Chem*. **2018**, 3675-3685.
21. S. X. Luo, K. M. Engle, X. F. Dong, A. Hejl, M. K. Takase, L. M. Henling, P. Liu, K. N. Houk and R. H. Grubbs, *ACS Catal.* 2018, **8**, 4600-4611.

View Article Online
DOI: 10.1039/D0DT02353A

22. M. Bieniek, C. Samojłowicz, V. Sashuk, R. Bujok, P. Śledź, N. l. Lugan, G. Lavigne, D. Arlt and K. Grela, *Organometallics*, 2011, **30**, 4144-4158.
23. R. Gawin, A. Makal, K. Wozniak, M. Mauduit and K. Grela, *Angew. Chem. Int. Ed.* 2007, **46**, 7206-7209.
24. K. Skowerski, P. Kasprzycki, M. Bieniek and T. K. Olszewski, *Tetrahedron*, 2013, **69**, 7408-7415.
25. J. M. Bates, J. A. M. Lummiss, G. A. Bailey and D. E. Fogg, *ACS Catal.* 2014, **4**, 2387-2394.
26. S. B. Garber, J. S. Kingsbury, B. L. Gray and A. H. Hoveyda, *J. Am. Chem. Soc.* 2000, **122**, 8168-8179.
27. M. A. Escobar, D. M. da Costa, O. S. Trofymchuk, C. G. Daniliuc, F. Gracia, F. M. Nachtigall, L. S. Santos, R. S. Rojas and A. R. Cabrera, *J Organomet. Chem*. 2018, **863**, 21-29.
28. J. V. Gavette, C. M. Klug, L. N. Zakharov, M. P. Shores, M. M. Haley and D. W. Johnson, *Chem. Commun.* 2014, **50**, 7173-7175.
29. F. Sce, G. Beobide, O. Castillo, I. de Pedro, S. Perez-Yanez and E. Reyes, *CrystEngComm*. 2017, **19**, 6039-6048.
30. G. Cavallo, P. Metrangolo, R. Milani, T. Pilati, A. Priimagi, G. Resnati and G. Terraneo, *Chem. Rev.* 2016, **116**, 2478-2601.
31. A. G. Dikundwar and T. N. G. Row, *Cryst. Growth Des*. 2012, **12**, 1713-1716.
32. A. Mukherjee, S. Tothadi and G. R. Desiraju, *Acc. Chem. Res*. 2014, **47**, 2514-2524.
33. L. Polito, M. Cravini, L. Poletti and L. Lay, *Syn. Commun*. 2006, **36**, 2203-2209.
34. D. J. Nelson, S. Manzini, C. A. Urbina-Blanco and S. P. Nolan, *Chem. Commun*. 2014, **50**, 10355-10375.
35. T. Vorfalt, K. J. Wannowius and H. Plenio, *Angew. Chem. Int. Ed.* 2010, **49**, 5533-5536.
36. I. W. Ashworth, I. H. Hillier, D. J. Nelson, J. M. Percy and M. A. Vincent, *Chem. Commun*. 2011, **47**, 5428-5430.

View Article Online
DOI: 10.1039/D0DT02353A

TOC one sentence

The reactivities of Hoveyda-Grubbs-type complexes are modulable through second-coordination sphere effects caused by a functional group in the ligand.